J. Fluid Mech. (1992), *vol.* 234, *pp.* 279–296
Printed in Great Britain

The production of constant-shear flow

By H. G. C. WOO AND J. E. CERMAK
Department of Civil Engineering, Colorado State University, Fort Collins, CO 80523, USA

(Received 25 March 1991 and in revised form 28 June 1991)

An effective and practical method of producing strong constant-shear flow with a low turbulence level in the laboratory has been developed. A pair of closely spaced shaped gauzes with the upstream gauze of non-uniform porosity and the downstream gauze of uniform porosity was used for the generation of the flow. The method presented can be generalized to specify the gauze shape and porosity distribution necessary to generate other velocity distributions desired in a duct flow.

1. Introduction

The simplest form of shear flow is constant-shear flow – a shear flow with a linear velocity distribution. This type of flow is best known as plane Couette flow. There is considerable interest in the generation of this type of flow for experimental purposes. The common practice for generating a constant-shear flow in the laboratory is by placing a shear-generating apparatus such as a tapered honeycomb (Kotansky 1966; Kiya, Tamura & Arie 1980), or a grid of parallel rods (Owen & Zienkiewicz 1957; Livesey & Turner 1964), or a curved gauge (Maull & Young 1973; Stansby 1976) in the flow. Upstream of the shear generator, the flow is generally uniform; downstream at the test section, the flow is sheared.

Once a constant-shear flow is generated, in addition to the viscous effects encroaching into the flow from the wall boundary layers, the relevant factors which affect the steadiness and decay of a velocity profile include local abrupt mean velocity changes and diffusion of momentum by turbulent mixing. Thus, for the practical requirement of having a persistent velocity profile,it is desirable to have a velocity distribution which is as linear as can possibly be achieved and also with a low level of turbulence intensity.

The honeycomb method presented by Kotansky (1966) can generate shear flows with quite smooth velocity variations and a low turbulence level. The disadvantage of this method is the significant technical difficulty involved in shaping the honeycomb block to a predetermined shape and making any corrections necessary to produce the desired velocity profile. The shear parameter λ is defined as

$$U/U_{\mathrm{m}}-1=\lambda(y/L-0.5). \tag{1.1}$$

Here, L (see figure 1) is the height of the shear flow, U is the velocity in the x-direction and the subscript m designates the value at mid-height of the flow. The shear parameters are 0.42 and 0.74 in the work of Kotansky (1966) and Kiya *et al.* (1980), respectively.

A representative work using a grid of parallel rods is that by Owen & Zienkiewicz (1957). Although their method is strictly applicable only to weakly sheared flows, close agreement with their theory was reported for a grid designed for a shear parameter of 0.43. By applying the method of Owen & Zienkiewicz, with some empirical corrections, Livesey & Turner (1964) produced two symmetrical shear

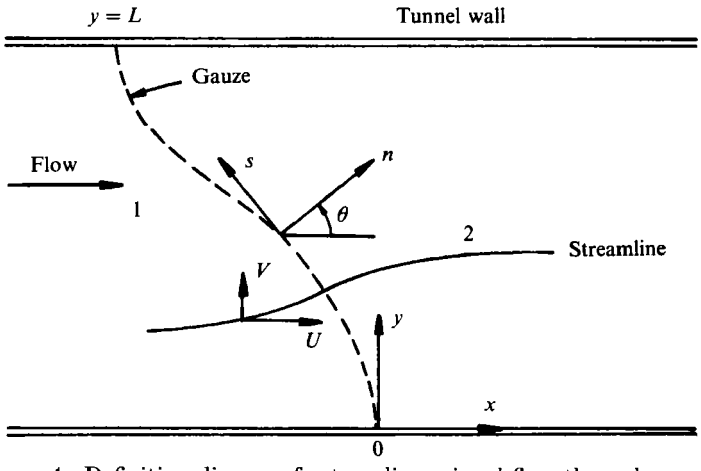

FIGURE 1. Definition diagram for two-dimensional flow through a gauze.

velocity profiles with shear parameters of 0.6 and 0.8. Technically, this method involving a grid of parallel rods is not too difficult to use. Through some empirical corrections, it could be used to generate quite strong shear flows. The disadvantage of this method is high turbulence intensities (Davies 1976).

The most generalized work on the subject of the production of a specific velocity distribution through the use of a spatial distribution of obstructions is perhaps the theory presented by Elder (1959). However, the practicality of obtaining analytical results by his method is limited owing to the mathematical complexity involved in solving the linearized equations. This obstacle was removed by Turner (1969) by means of a computational scheme which used relatively simple iterative techniques. The generation of a constant-shear flow with $\lambda = 0.35$ was among the problems analysed by Turner. By using a gauze with uniform porosity shaped according to the computed solutions, the results were found to be in satisfactory agreement. Maull (1968) modified the theoretical work of Elder and generated (also by means of a curved gauze with uniform porosity) a constant-shear flow with $\lambda = 0.4$ and turbulence intensities around 0.5%. This device of Maull was later used by Maull & Young (1973), Mair & Stansby (1975) and Stansby (1976) for their studies.

The study presented herein was undertaken to develop an effective and practical method for the production of constant-shear flows. The emphasis is on linearity of the velocity distribution and low turbulence level, which are necessary for many laboratory investigations. The analysis and considerations involved in the manufacture of shear-flow generators, in certain respects, represent extensions of the work of Vahl Davis (1957), Elder (1959) and Turner (1969). An insightful overview regarding flow through screens has been given by Laws & Livesey (1978).

Constant-shear flow properties for various gauze configurations are presented in the following order: (i) single gauze, uniform porosity; (ii) single gauze, non-uniform porosity; (iii) pair of gauzes, both uniform porosity; and (iv) pair of gauzes, non-uniform followed by uniform porosity.

2. Gauze parameters and boundary conditions

Initially, it is useful to restate some of the main steps of the analytical work of Vahl Davis (1957) and Elder (1959). A gauze of arbitrary shape, described by $x = f(y)$, is situated in a two-dimensional channel of height L (figure 1). The gauze is

regarded as a surface of discontinuity in velocity, pressure, and vorticity. The effect of viscosity is neglected except in the immediate vicinity of the gauze. Further, the flow is considered to be incompressible.

2.1. *Gauze parameters*

When flow passes through a gauze, there are instantaneous changes in static pressure, which are given by the pressure drop (or resistance) coefficient K, and changes in tangential velocity, which are given by the deflection (or lift) coefficient B. These two parameters are necessary to predict the aerodynamic characteristic of a gauze. The pressure drop coefficient K is defined by

$$K = \Delta p/(0.5\rho U_n^2), \tag{2.1}$$

where Δp is the static pressure drop across the gauze, ρ is the fluid density, and U_n is the local velocity component normal to the gauze surface. The deflection coefficient B is defined by

$$B = (V_{s1} - V_{s2})/V_{s1}, \tag{2.2}$$

where V_s is the tangential velocity. The subscripts 1 and 2 represent upstream and downstream conditions, respectively (figure 1). Thus, B is a measure of the amount by which a gauze refracts a streamline which is at a given incident angle to it.

The gauze characteristics K and B are assumed to be independent of the Reynolds number and dependent only on the physical properties of the gauze. For a square-mesh wire gauze, Elder (1959) assumed that

$$K = [(1-\beta)/\beta]^2, \tag{2.3}$$

where β is the fractional open area of the gauze, and that B is related to K by

$$B = 1-(1+K^{\frac{1}{2}})^{-\frac{1}{2}}. \tag{2.4}$$

2.2. *The linearized boundary conditions at the gauze*

The effective loss coefficient γ, as given by Vahl Davis (1957), is

$$\gamma = K\cos^2\theta. \tag{2.5}$$

It is a function of K and the angle θ between the normal to the gauze and the unperturbed flow direction (figure 1). If the variations of θ and resistance γ across the gauze are both small, then we can write

$$\gamma = \gamma_0[1+s(y)], \tag{2.6}$$

where γ_0 is the mean effective loss coefficient which is a constant determined by both the shape and physical properties of the gauze. Note that $s(y)$ is a function of both K and θ.

The equations relating the velocity changes to the gauze properties, as given by Vahl Davis (1957) and Elder (1959), are

$$u-u^* = \gamma_0(q-1)+0.5\gamma_0 s, \tag{2.7}$$

and

$$\hat{u}_1 = \hat{u}_2 = q, \tag{2.8}$$

$$BqT = (1-B)v_1 - v_2, \tag{2.9}$$

where

$$u = \frac{U_{\infty 1}}{\bar{V}}, \quad u^* = \frac{U_{\infty 2}}{\bar{V}}, \quad q = \frac{U}{\bar{V}}, \quad \hat{u}_1 = \frac{U_1}{\bar{V}}, \quad \hat{u}_2 = \frac{U_2}{\bar{V}},$$

$$T = \tan\theta, \quad v_1 = \frac{V_1}{\bar{V}}, \quad v_2 = \frac{V_2}{\bar{V}}.$$

Here, $\bar{V}$ (equal to U_m in the present study) is a suitable mean velocity for non-dimensionalizing the equations and q is the local flow velocity at the gauze surface. The mean velocity in the y-direction is designated by V. The suffix ∞ represents a value distant from the plane of the gauze.

3. A single gauze in a two-dimensional channel

3.1. *Governing equations*

If the gauze produces a perturbation ψ' to the undisturbed stream function ψ_∞ such that $\psi = \psi_\infty + \psi'$, provided that the perturbation is small (note that this assumption is not necessary in the case of constant-shear flows), then

$$\nabla^2 \psi' = 0. \tag{3.1}$$

A finite solution of (3.1), which satisfies the boundary conditions at the walls and the gauze (§2.2) and the assumption that the gauze is everywhere nearly coincident with the plane $x = 0$ as given by Elder (1959), is

$$u^* - 1 = A(u-1) - 0.5(1-A)\, s + E \sum_{n=1}^{\infty} \alpha_n \cos n\omega, \tag{3.2}$$

where

$$A = \frac{2-\gamma_0-B+\gamma_0 B}{2+\gamma_0-B}, \quad E = \frac{\gamma_0}{2+\gamma_0-B}, \quad \omega = \frac{\pi y}{L}, \quad \sum_{n=1}^{\infty} \alpha_n \sin n\omega = BT.$$

Equation (3.2) is a result relating the upstream and the downstream velocity distributions, the aerodynamic coefficients, and the geometrical shape of the gauze.

By using a transformation technique discussed by Hardy & Rogosinski (1944), here designated as H and H^*, to overcome the difficulty of evaluating α_n, Elder (1959) was able to write (3.2) as

$$(u^* - 1) - A(u-1) + 0.5(1-A)\, s = E\, H[BT], \tag{3.3a}$$

or as

$$BT = H^*[(u^* - u)/E + (2-B)\,(u-1) + 0.5(2-B)\, s]. \tag{3.3b}$$

The mathematical difficulty of obtaining analytical solutions to (3.3) even for some carefully chosen problems are tremendous. Turner (1969) took a numerical approach by presenting a computational scheme to solve this equation.

3.2. *Generation of constant-shear flow with a curved gauze of uniform porosity*

Figure 2 shows some computed gauze shapes following the iterative procedures of Turner (1969). The calculations were based on the physical properties of a selected fabric mesh gauze which was used in the manufacture of shear-flow generators. The square-mesh gauze has a density of 30 mesh/cm. Each strand is about 0.15 mm in diameter. Thus, it has a porosity β of 0.32 and resistance coefficient K of 4.52.

Throughout the course of this study, more than a dozen shear-flow generators were manufactured with four basic gauze shapes, which were calculated to have shear flow parameters $\lambda^* = 0.4$, 0.6, 0.8, and 0.95 as shown in figure 2. They were installed in an open-return-type wind tunnel which had a 61 cm square cross-section. The gauzes were placed at the entrance of the wind tunnel immediately following a fine honeycomb block of 5 cm thickness used to secure a uniform, low-turbulence approach flow. The gauze was glued to Plexiglas frames which were then bolted to the sidewalls. Tension on the gauze was applied mainly in the lateral direction.

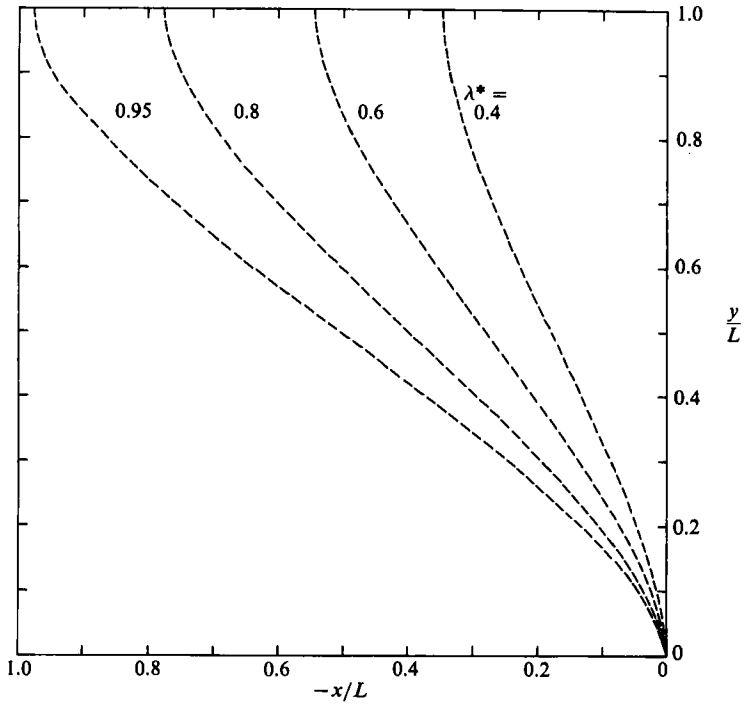

FIGURE 2. The gauze shape required to produce a constant-shear flow. $\beta = 0.32$, $K = 4.52$.

Measurements of the vertical velocity distribution were made at $x/L \geqslant 1.7$, where the shear flows were fully developed. Some of these results are shown in figure 3. The velocity profiles are all quite smooth. The local turbulence intensity (r.m.s. of the fluctuation velocity/the local mean velocity) is approximately 0.3%, except in the wall boundary-layer regions where it is higher. Experimental values of the shear parameter match those of theoretical predictions very well up to $\lambda^* = 0.6$ as shown in figure 4; the bars represent the range of scatter of the data. For the $\lambda^* = 0.6$ gauze, spanwise along the gauze, $\theta_{\max} = 36.71°$. This result for curved gauzes is in close agreement with the results for linear gauzes of Vahl Davis (1957) and Elder (1959). Thus, this small-perturbation solution, specifically in terms of refraction of the streamline by a gauze, applies for θ up to 40°. As the shear parameter increases beyond 0.6, the discrepancy between theoretical predictions and experimental results increases. A departure of the velocity distribution from linearity in the upper and lower regions where $B\tan\theta$ varies rapidly is also seen. These are the regions where Maull (1968) found it necessary to modify the gauze shape in an empirical fashion in order to generate a flow suitable for his studies.

3.3. *Generation of constant-shear flow with a curved gauze of non-uniform porosity*

In the preceding section, the calculation of the gauze shape required to generate a designated constant-shear flow was based on the assumption that the physical properties of the gauze are uniform. Therefore, spanwise variation of the amount by which the gauze refracts the streamline is dependent only on the change of the gauze shape; i.e. on $\theta(\omega)$. In this section, additional flow control is introduced by suitable variation of the gauze porosity $\beta(\omega)$, and thus $K(\omega)$, $B(\omega)$, and $\gamma(\omega)$.

A solution to the problem of producing a constant-shear flow with a gauze of non-uniform porosity can be obtained in two steps. The first is to obtain the gauze shape

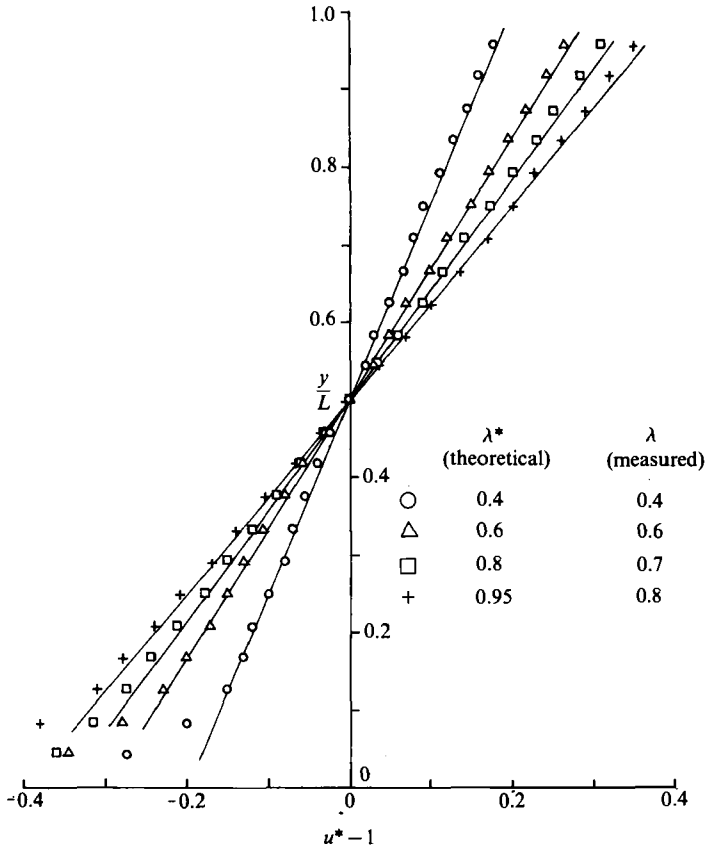

FIGURE 3. The velocity profile downstream of a curved gauze of uniform porosity.

required to produce a shear flow with shear parameter λ^* with the assumption of uniform porosity as has been discussed in §3.2. The second step is to increase the shear parameter by an amount $\Delta\lambda$ to a new level by varying the porosity across the gauze. Physically, this can be achieved in the laboratory by spraying an acrylic resin onto the gauze. The required distribution of K for the gauze can be calculated from (3.3) by a numerical iterative procedure similar to that introduced by Turner (1969) for the gauze shape. An additional boundary condition, $K \geqslant K_{\text{plain gauze}}$, was imposed in the calculations. It should be emphasized that during the calculations in step 2 the shape of the gauze $\theta(\omega)$ is determined from the calculation in the first step. The theoretical distributions of K that are required for the $\lambda^* = 0.4$ and the $\lambda^* = 0.6$ gauzes (figure 2) to increase the shear parameter to 0.6 and 0.8, and 0.8 and 1.0, respectively, are shown in figures 5(*a*) and 5(*b*).

With the gauzes installed in a wind tunnel, direct measurement of the resistance coefficient variation is impractical, especially in the double-gauze situation which will be discussed in §4.3. Therefore, the necessary adjustments of porosity distribution for both the single- and double-gauze cases were carried out by direct measurement of the velocity profile downstream using the theoretical predictions as a guide. The extent of streamline displacement at a particular location along the gauze was obtained by visualization with smoke tracer. Measurements of the resistance coefficient were performed after dismantling the gauze from the supporting frames. Any designated position on the gauze was then inserted in the middle of a

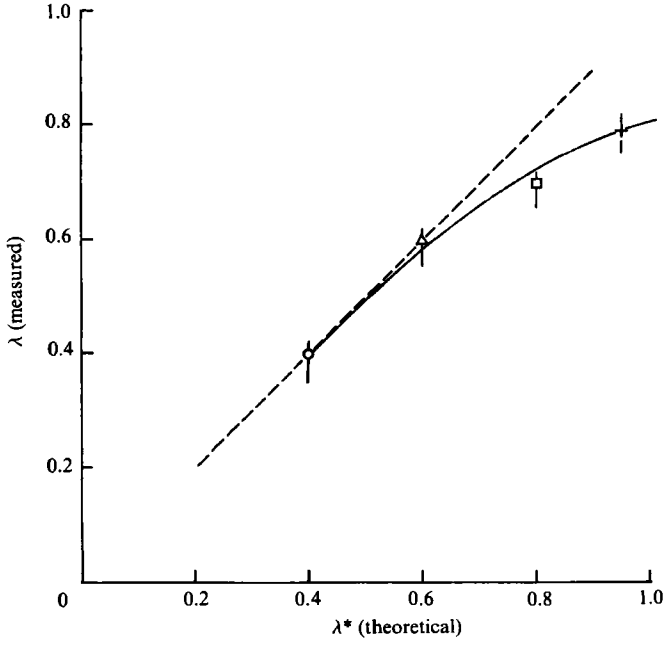

FIGURE 4. A comparison of the theoretical and experimental shear parameters for a single gauze of uniform porosity.

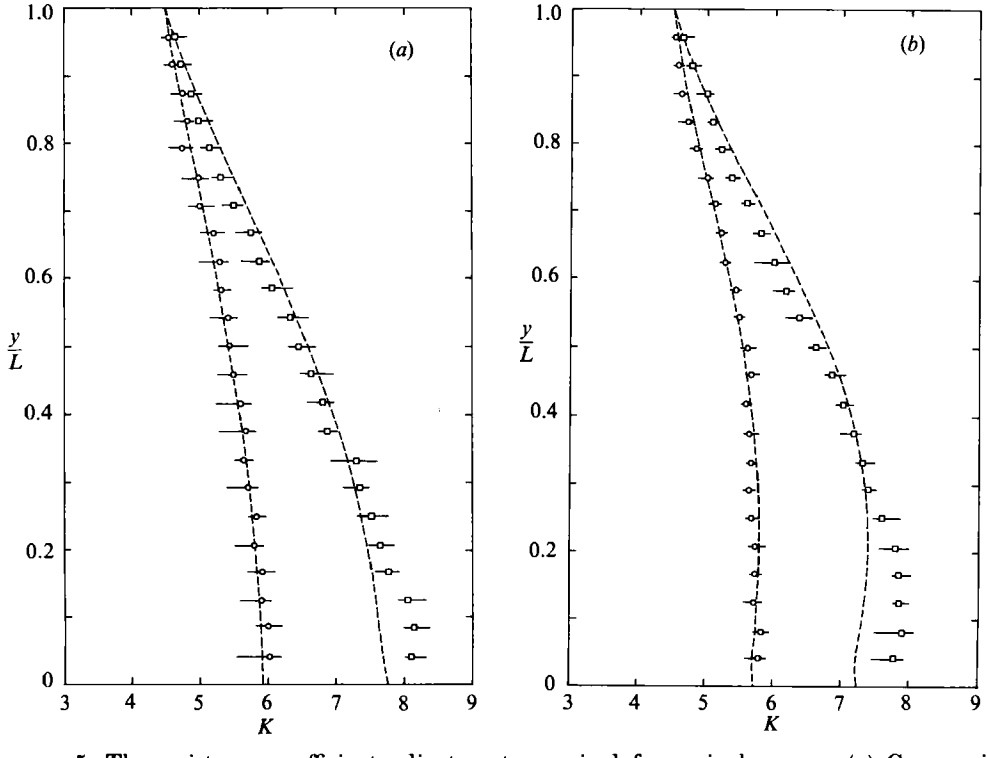

FIGURE 5. The resistance coefficient adjustments required for a single gauze. (*a*) Gauze with $\lambda^* = 0.4$: ———, theoretical prediction; measured value: –○–, increase λ to 0.6; –□–, increase λ to 0.8. (*b*) Gauze with $\lambda^* = 0.6$: – – –, theoretical prediction; measured value: –○–, increase λ to 0.8; –□–, increase λ to 1.0.

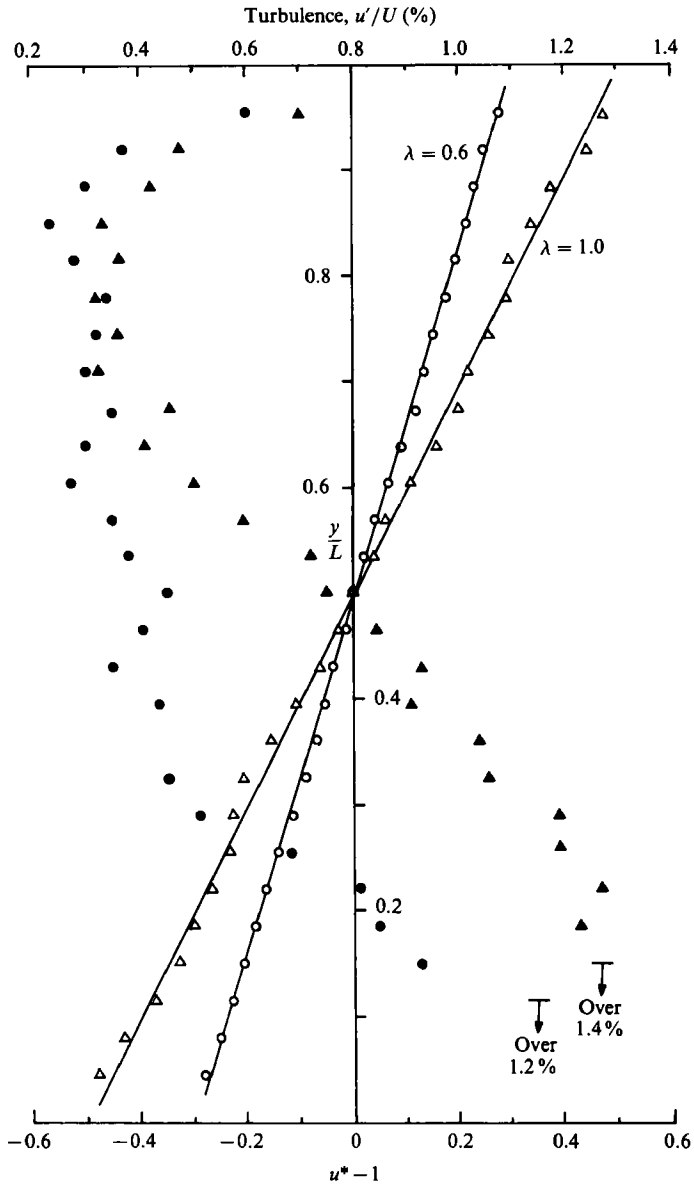

FIGURE 6. The velocity and turbulence intensity profiles downstream of a curved gauze of non-uniform porosity. $\lambda^* = 0.4$: ○, mean velocity; ●, turbulence intensity. $\lambda^* = 0.6$: △, mean velocity; ▲, turbulence intensity.

pipe flow with 1.27 cm in diameter and Δp was measured. U_n was set at 3 m/s at which the Reynolds-number effect on K disappears. The experimental results are compared with the theoretical predictions in figure 5 (a, b). Close agreement is found in the cases of the $\lambda^* = 0.4$ gauze with an increase in the shear parameter to 0.6, and the $\lambda^* = 0.6$ gauze with an increase to 0.8. For the cases of the $\lambda^* = 0.4$ gauze with an increase in the shear parameter to 0.8 and the $\lambda^* = 0.6$ gauze with an increase to 1.0, the experimental results generally follow the trends of theoretical prediction and the comparisons are favourable.

The flow downstream of the gauze was found to be very sensitive to treatment of the gauze. Therefore, spraying to change the porosity of a gauze must be carried out in a careful manner. Any local abrupt variation of the spray (the porosity) can generate large-scale eddies and result in abrupt mean velocity changes as well as a high turbulence level as shown in the case of the $\lambda^* = 0.6$ gauze increasing the shear parameter to 1.0 (figure 6). Unfortunately, technically it is rather difficult to change the gauze porosity uniformly in the lateral direction and smoothly varying in the vertical direction. Attempts to overcome this shortcoming led to the concept of placing a second gauze of the same shape but with uniform porosity immediately after the first gauze. Any local non-smooth effect and high turbulence intensity caused by the first gauze should be quite effectively attenuated by the second gauze if the second gauze is fine and uniform. Meanwhile, the second and third terms on the right-hand side of (3.2) for the second gauze should have the overall effect of increasing the shear strength of the flow generated.

4. Two gauzes placed in series

4.1. *Governing equations*

Consider two gauzes placed in series, gauze A is located at $x = 0$ and gauze B at $x = x_0$; denote the region upstream of A as region 1, downstream of B as region 3, and in between A and B as region 2. The general solution of the perturbation stream functions has the form

$$\frac{\psi'}{LV} = \sum_{n=1}^{\infty} \frac{1}{n\pi} (P_n \, \mathrm{e}^{n\pi x/L} - Q_n \, \mathrm{e}^{-n\pi x/L}) \sin \frac{n\pi y}{L}. \tag{4.1}$$

By definition of the problem, ψ' approaches 0 as x approaches $\pm\infty$. Therefore, we have in region 1:

$$\frac{\psi_1}{LV} = \frac{\psi_{\infty 1}}{LV} + \sum_{n=1}^{\infty} \frac{1}{n\pi} P_{1n} \, \mathrm{e}^{n\pi x/L} \sin \frac{n\pi y}{L}; \tag{4.2}$$

region 2:

$$\frac{\psi_2}{LV} = \frac{\psi_{\infty 2}}{LV} + \sum_{n=1}^{\infty} \frac{1}{n\pi} (P_{2n} \, \mathrm{e}^{n\pi x/L} - Q_{2n} \, \mathrm{e}^{-n\pi x/L}) \sin \frac{n\pi y}{L}; \tag{4.3}$$

and region 3:

$$\frac{\psi_3}{LV} = \frac{\psi_{\infty 3}}{LV} - \sum_{n=1}^{\infty} \frac{1}{n\pi} Q_{3n} \, \mathrm{e}^{-n\pi x/L} \sin \frac{n\pi y}{L}. \tag{4.4}$$

Let $\xi_n = n\pi x_0/L$, $u_{\infty 1} = u$ and $u_{\infty 3} = u^*$. The linearized boundary conditions at the gauzes (§2.2) then yield the following relationships:

$$B_{\mathrm{A}} T_{\mathrm{A}} = \sum_{n=1}^{\infty} G_n \sin n\omega, \tag{4.5}$$

$$\gamma_{\mathrm{A}}(u-1) + 0.5\gamma_{\mathrm{A}} s_{\mathrm{A}} = \sum_{n=1}^{\infty} H_n \cos n\omega, \tag{4.6}$$

$$B_{\mathrm{B}} T_{\mathrm{B}} = \sum_{n=1}^{\infty} M_n \sin n\omega, \tag{4.7}$$

$$\gamma_{\mathrm{B}}(u^*-1) + 0.5\gamma_{\mathrm{B}} s_{\mathrm{B}} = \sum_{n=1}^{\infty} L_n \cos n\omega, \tag{4.8}$$

where $(1-B_A)P_{1n}-P_{2n}-Q_{2n}=G_n$, $(1+\gamma_A)P_{1n}-P_{2n}+Q_{2n}=H_n$,

$(1-B_B)(P_{2n}e^{\xi_n}+Q_{2n}e^{-\xi_n})-Q_{3n}e^{-\xi_n}=M_n$, $(1-\gamma_B)Q_{3n}e^{-\xi_n}+P_{2n}e^{\xi_n}-Q_{2n}e^{-\xi_n}=L_n$.

Assume that the approaching flow is uniform, i.e. $u-1=0$, express the downstream velocity field in terms of a trigonometric series,

$$u^*-1=\sum_{n=1}^{\infty}F_n\cos n\omega,$$

and define $\eta_n=\coth\xi_n$ and $\zeta_n=\cosh\xi_n$, then it can be shown that

$$F_nf_n+H_nh_n+L_nl_n+G_ng_n+M_nm_n=0 \tag{4.9}$$

where

$$f_n=[(1-B_A)(1-B_B)(1-\gamma_B)+(1+\gamma_A)]\eta_n+[(1-B_B)(1+\gamma_A)(1-\gamma_B)+(1-B_A)]$$

$$h_n=[(1-B_A)(1-B_B)(1-\gamma_B)+1]\eta_n+\gamma_B(1-B_A)(1-B_B)\zeta_n$$
$$+[(1-B_A)+(1-B_B)(1-\gamma_B)],$$

$$l_n=[(1-B_A)(1-B_B)+(1+\gamma_A)]\eta_n-\gamma_A\zeta_n+[(1-B_B)(1+\gamma_A)+(1-B_A)],$$

$$g_n=-\gamma_A(1-B_B)(1-\gamma_B)\eta_n-\gamma_B(1-B_B)(1+\gamma_A)\zeta_n-\gamma_A,$$

$$m_n=-\gamma_A(1-\gamma_B)\zeta_n-\gamma_B(1+\gamma_A)\eta_n-\gamma_B(1-B_A).$$

Equation (4.9) must hold for $0\leqslant y\leqslant L$.

4.2. *The effect of spacing between two gauzes on the downstream velocity*

For a gauze of uniform porosity, if the restrictions inherent in the linearized theory are properly observed, it can be shown that the computed gauze shape is practically unchanged if the resistance variation term $s(\omega)$ is neglected (see also Turner 1969). Therefore, with uniform approach flow, for a pair of identical gauzes of uniform porosity, we have: $G_n=M_n$, $H_n=0$, and (4.8) becomes

$$\gamma_B(u^*-1)=\sum_{n-1}^{\infty}L_n\cos n\omega. \tag{4.10}$$

Equation (4.9) and the related coefficients can also be simplified accordingly.

With the gauze parameters γ_0 and $T(\omega)$ obtained from the numerical scheme of Turner (1969), the downstream velocity distribution u^*-1 as a function of the distance x_0/L between gauzes can be calculated from a simplified form of (4.9). To check the theoretical predictions, a series of experiments were performed with two separate pairs of gauzes that have shapes like those of $\lambda^*=0.4$ and 0.6 in figure 2 at various distances apart. These results are shown in figure 7 (*a*, *b*). Comparisons of the theoretical predictions and test results generally show that better agreement is obtained in the upper part of the flow than the lower part, and the $\lambda^*=0.4$ gauze is better than $\lambda^*=0.6$. That both the theoretical predictions and experimental results for the velocity profile (compare with figure 3) are not linear is quite obvious.

Owing to mutual interference, a pair of gauzes that individually can produce (at least theoretically) a constant-shear flow may no longer be able to do so when they are placed together in series. Namely, the shape required for a pair of identical gauzes to generate a particular constant-shear flow may differ from the shape required for

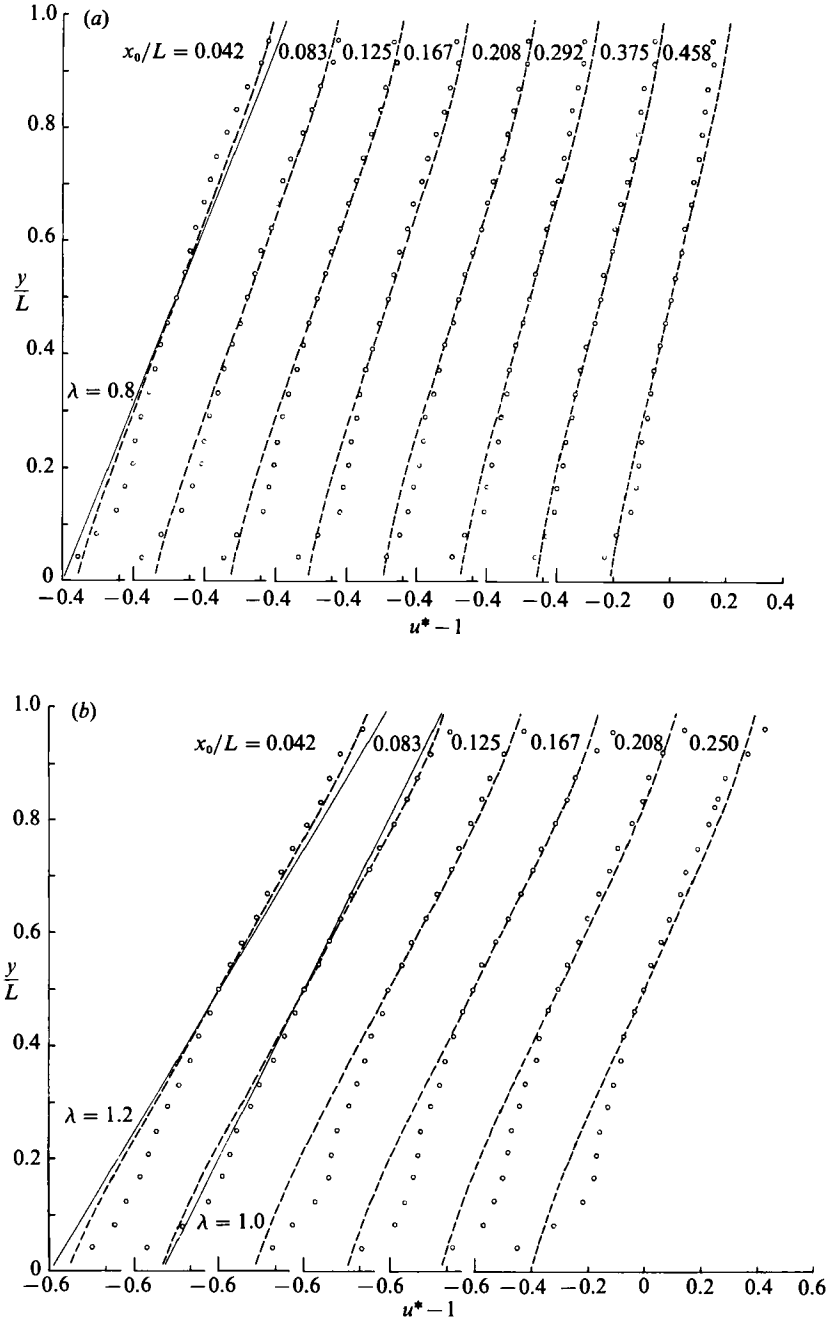

FIGURE 7. The velocity profile downstream of a pair of curved gauzes of uniform porosity at various distances apart. (*a*) $\lambda^* = 0.4$; (*b*) $\lambda^* = 0.6$. ---, Theoretical result; ○, measured value.

a single gauze. As the separation of the pair, x_0/L, approaches zero, it can be shown that (4.9) reduces to (3.2) with $E = 2\gamma(2-B)/(2+2\gamma-2B+B^2)$. This is an asymptotic case where theoretically the resulting flow downstream is linear. As x_0/L approaches infinity, the result given by (4.9) is the same as by using (3.2) twice or by using (3.2) with $E = (4\gamma-2B\gamma+B\gamma^2)/(2+\gamma-B)^2$. this is another asymptotic case where the

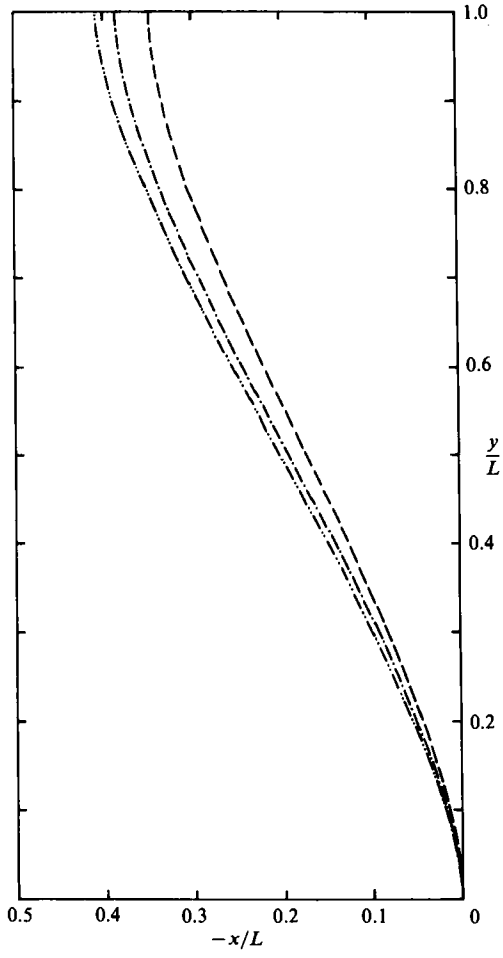

FIGURE 8. The required adjustments of gauze shape for a pair of identical gauzes to produce a constant-shear flow. —·—·—, double gauzes separated by $x_0/L = 0.042$ to produce a shear flow with $\lambda = 0.8$; —··—··—, double gauzes separated by $x_0/L = 0.083$ to produce a shear flow with $\lambda = 0.8$; – – –, $\lambda^* = 0.4$.

resulting flow downstream is also linear. In between these two cases, $0 < x_0/L < \infty$, the nonlinear effect varies. This effect can be seen in figure 7 (*a*, *b*). In principle, based on (4.9), one could calculate the required adjustments of gauze shape in order to produce a shear flow with a linear velocity distribution downstream, as given in two examples shown in figure 8. This approach has not been adopted in this study because of the obvious reason that adjustment of the gauze shape, especially minor corrections, is far more difficult and cumbersome than adjustment of the gauze porosity.

One of the difficulties experienced in the wind-tunnel experiments is to impose proper tension, mainly laterally and slightly vertically on the gauze. Note that the tension imposed on the gauze needs to balance that developed by wind pressure on it under test conditions in order to maintain its designed section shape. Any variation or discrepancy after each installation or adjustment of the gauze can cause changes in the gauze shape and result in test errors. Despite these experimental difficulties and with some approximation to the λ-value for the velocity profile, figure 9 shows

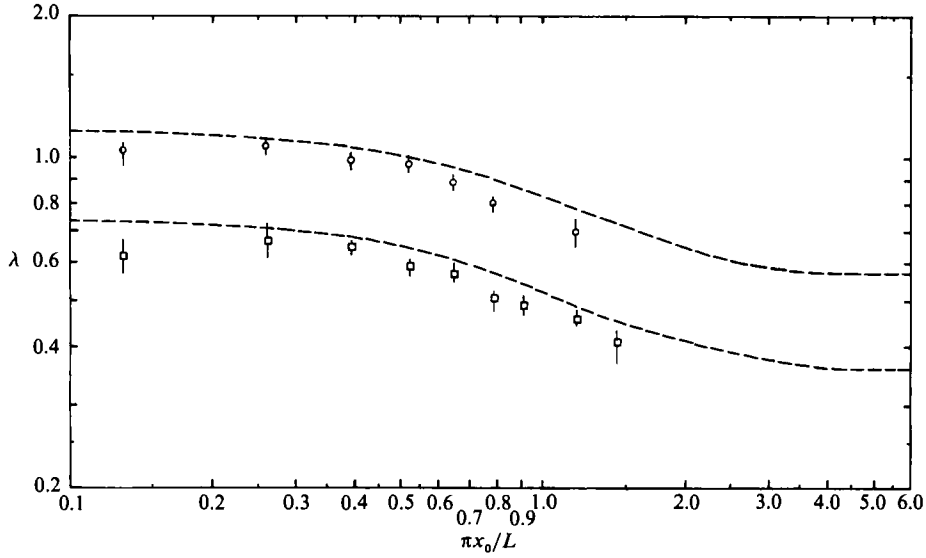

FIGURE 9. A comparison of the shear parameter for a pair of curved gauzes of uniform porosity at various distances apart. ---, Theoretical prediction. Measured value: ⏀, gauze with $\lambda^* = 0.4$; ◊, gauze with $\lambda^* = 0.6$.

that the shear parameters obtained from the measurements generally follow the trends predicted by the theory but the values are consistently lower. The contribution of the upstream gauze in increasing the shear-flow strength diminishes rather quickly as the distance between the gauzes increases and practically disappears at $\pi x_0/L =$ 2.2 for the $\lambda^* = 0.4$ gauzes and 2.6 for the $\lambda^* = 0.6$ gauzes. Beyond these distances, the upstream gauzes have negative contribution. In fact, if x_0/L is large enough, it can be assumed that the gauzes do not interfere with each other. Under this circumstance, (3.2) can be applied separately for the upstream and downstream gauzes. The factor A in (3.2) represents the manner in which a gauze attenuates the velocity unevenness. Depending on the value being positive or negative, the sense of reduction in the velocity variation may be reversed. In the two cases shown in figure 9, A has negative values. Therefore, if the upstream gauze is replaced with a gauze that generates weaker shear flow or even shear flow with negative shear parameter, it would result in a stronger shear flow generated downstream. Under certain conditions A can be positive. In this case, as x_0/L increases, the shear strength decreases, but there will be no crossover point and the upstream gauze will always have a positive contribution. The wind tunnel used in this study has very limited test length; therefore, measurements could not be carried out beyond the crossover points. The resulting calculated shear strength as shown in figure 9 reaches the asymptotic values of 0.36 and 0.56, respectively.

4.3. *Generation of constant-shear flow with a pair of curved gauzes with identical shape, with the upstream one of non-uniform porosity and the downstream one of uniform porosity*

With a second gauze of uniform porosity and the same shape placed immediately downstream of the first gauze, the required adjustments in porosity distribution for the first gauze in order to generate a shear flow with the same shear strength or increase the shear strength to a new value, can be calculated from a simplified form

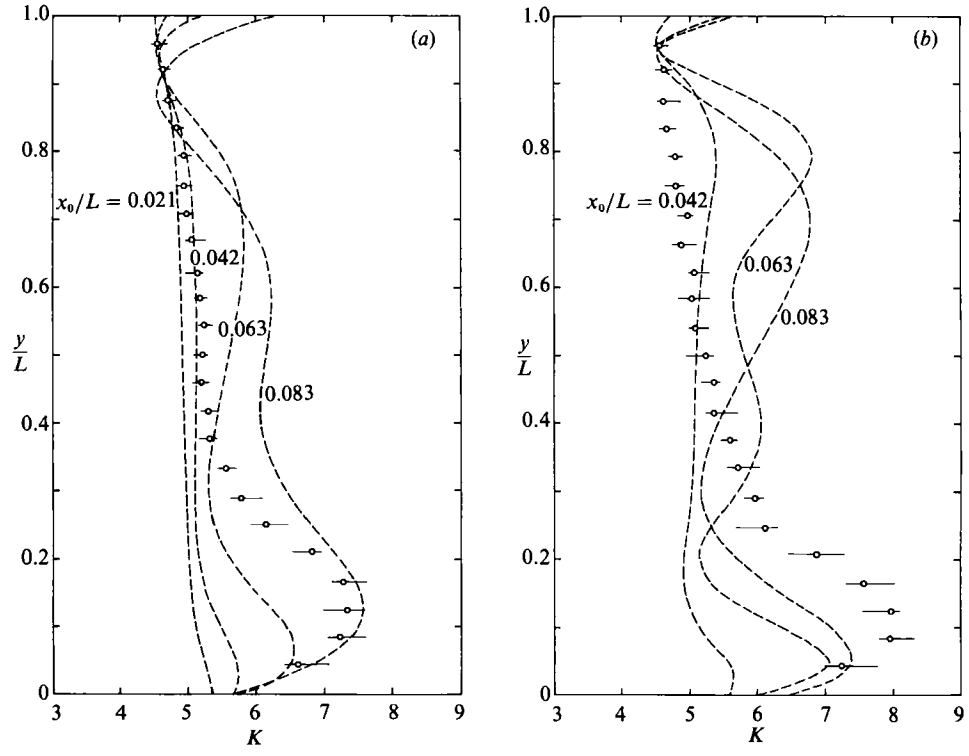

FIGURE 10. The resistance coefficient adjustments required for the upstream gauze in a double-curved-gauze situation. (*a*) A pair of $\lambda^* = 0.4$ gauzes: ---, theoretical prediction; measured value: -○-, at $x_0/L = 0.042$ to increase λ to 0.8. (*b*) A pair of $\lambda^* = 0.6$ gauzes: ---, theoretical prediction; measured value: -○-, at $x_0/L = 0.042$ to increase λ to 1.2.

of (4.9). Note that with the upstream gauze of varying porosity and the downstream gauze of uniform porosity, (4.6) becomes

$$0.5\gamma_A s_A = \sum_{n=1}^{\infty} H_n \cos n\omega, \tag{4.11}$$

and (4.8) reduces to (4.10). Note also that since $B_A \neq B_B$, $G_n \neq M_n$. An iterative technique using the quasi-Newtonian method for nonlinear optimization (Dennis & Schnabel 1983) was applied in the calculations. Again the physical restriction that $K \geqslant K_{\text{plain gauze}}$ was imposed.

Figure 10(*a*, *b*) shows examples of how the required distributions of K for the upstream gauze vary with the distance between the gauzes. One general conclusion based on these theoretical predictions is that the second gauze should be placed as close as possible to the first one. This is because the adjustments of the resistance coefficient needed for the first gauze increase rather quickly as x_0/L increases. By placing two gauzes closer together, changes of porosity of the first gauze become more effective. However, one has to be aware that in practice two gauzes must not be placed too close together, since then the effective porosity of the two gauzes becomes non-uniform because of non-uniform matching of wire locations in the two gauzes: some wires overlap, some overlap partially, some not at all. This results in complex interference fringe patterns over the gauzes that cause perturbations in the velocity distribution downstream.

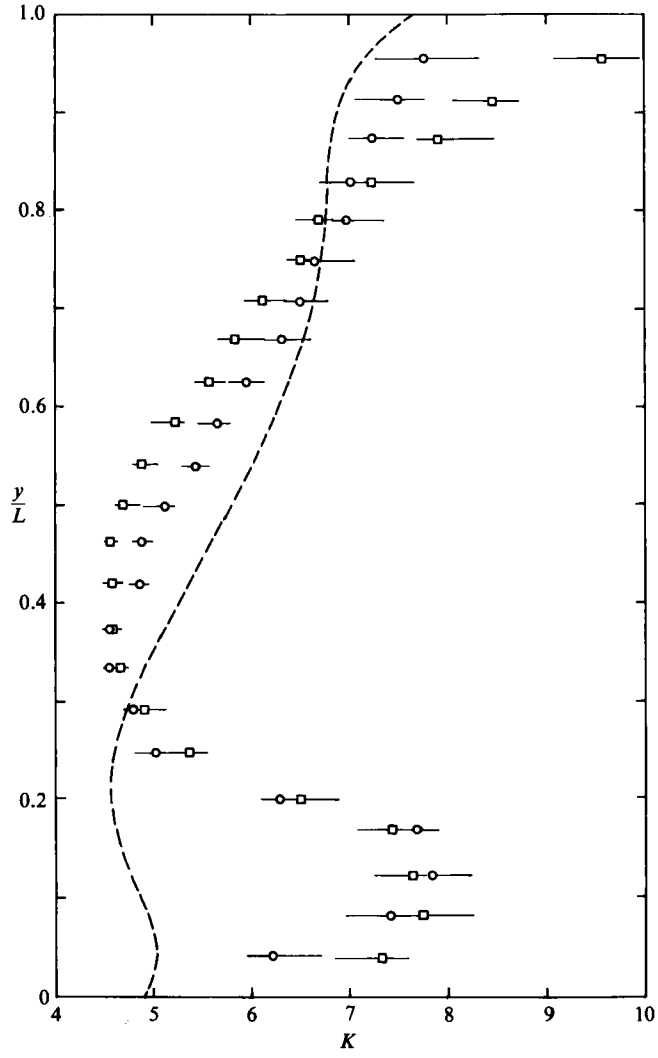

FIGURE 11. The resistance coefficient adjustments required for the upstream gauze in a double-curved-gauze situation. – – –, Theoretical prediction for a pair of $\lambda^* = 0.6$ gauzes at $x_0/L = 0.083$ to adjust λ into 1.0; Measured value. –○–, a pair of $\lambda^* = 0.6$ gauzes at $x_0/L = 0.083$ to adjust λ to 1.0; –□–, a pair of $\lambda^* = 0.95$ gauzes at $x_0/L = 0.042$ to adjust λ to 1.5.

By comparing figure 10(*a*, *b*) to figure 5(*a*, *b*), the effect of mutual interference between a pair of gauzes on the distribution of the resistance coefficient becomes obvious. As the distance between the gauzes diminishes, say $x_0/L < 0.042$ for the cases investigated, a pair of gauzes theoretically behaves more like a single gauze. This is reflected in the calculated results that the velocity profiles generated become more linear and the required variations of K become similar in shape to those for a single gauze shown in figure 5. This is more obvious for the $\lambda^* = 0.4$ gauzes in which the small streamline displacement assumption is more valid than for the $\lambda^* = 0.6$ gauzes.

Experimental results on resistance coefficient distributions for a pair of $\lambda^* = 0.4$ gauzes separated by $x_0/L = 0.042$ to increase the shear parameter to 0.8 and a pair of $\lambda^* = 0.6$ gauzes which were also separated by $x_0/L = 0.042$ to increase the shear

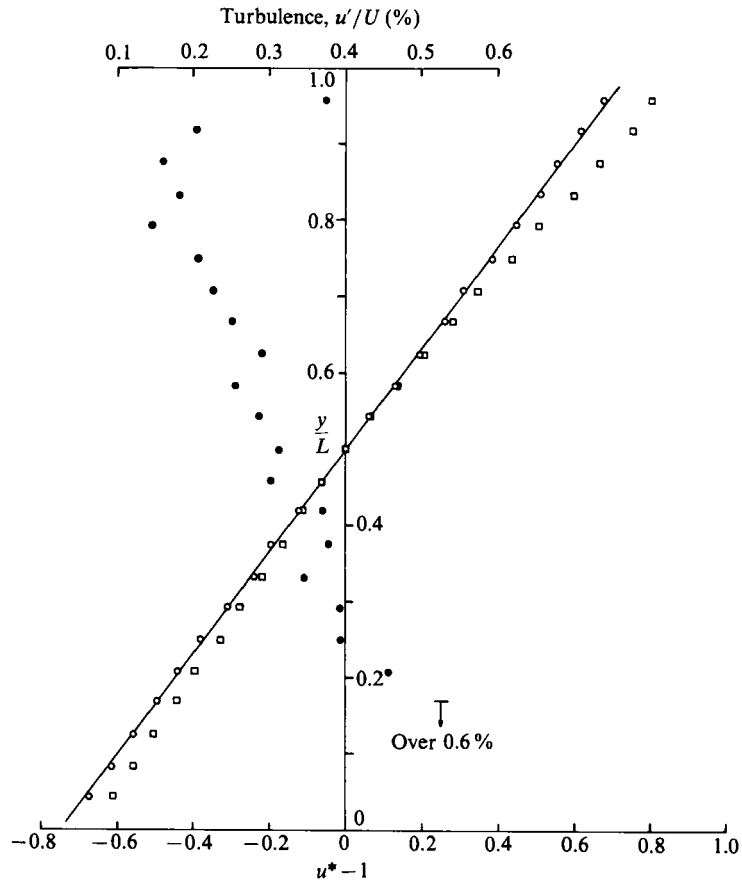

FIGURE 12. The velocity and turbulence intensity profiles downstream of a pair of curved gauzes that have $\lambda^* = 0.95$ at $x_0/L = 0.042$. Measured value: □, mean velocity with the upstream gauze of uniform porosity; ○, mean velocity, and ●, turbulence intensity with the upstream gauze of non-uniform porosity.

parameter to 1.2 are shown together with the theoretical predictions in figures 10(*a*) and 10(*b*), respectively. Quantitative agreement between the theoretical predictions and experimental results is rather poor. This result was expected because large discrepancies, especially in the lower part of the flow, already existed in the predicted and actual velocity profiles for the uniform-porosity situations (figure 7*a*, *b*). The actual variations of K are generally similar in distribution to those for the single-gauze cases (figure 5*a*, *b*). Qualitative agreement is considered fair for the $\lambda^* = 0.4$ gauzes (figure 10*a*).

Figure 11 shows both the predicted and actual distribution of K required for a pair of $\lambda^* = 0.6$ gauzes separated by $x_0/L = 0.083$ to adjust the shear parameter to 1.0. In this case velocities in the upper and lower parts of the flow need to be reduced (see figure 7*b*) in order to achieve this objective. In a similar situation in which a pair of $\lambda^* = 0.95$ gauzes were placed $x_0/L = 0.042$ apart (the velocity profile is shown in figure 12), by changing the resistance coefficient of the upstream gauze in a similar manner (also shown in figure 11), a case of constant-shear flow with $\lambda = 1.5$ and turbulence intensities around 0.2% to 0.4% was produced as shown in figure 12.

The lower limit on the turbulence intensity attainable by the use of a damping gauze is determined by the fineness and uniformity of the gauze and is unrelated to

the porosity. Therefore, by using a finer mesh gauze with the same physical characteristics and porosity, a shear flow with the same strength but with lower turbulence level could be produced.

By using this technique of double-curved gauzes, a few cases of strong constant-shear flows ($\lambda = 1.5$ to 1.6) with low turbulence intensities have been successfully produced in the laboratory for studies reported by Woo, Cermak & Peterka (1989). The streamlines are essentially parallel at the test section with the constant shear extending to the lower velocity end without evidence of separation. The flow characteristics are very stable and do not change significantly with the variation of flow speed in the test section.

5. Concluding remarks

An effective and practical method of generating strong constant-shear flow with a low turbulence level has been developed.A pair of closely spaced curved gauzes with the upstream gauze of varying porosity and the downstream gauze of uniform porosity was used. The required distribution of porosity for the upstream gauze was obtained by spraying with acrylic-resin spray. Adjustments to the downstream flow can be made quite easily by selective spraying of the first gauze. The significant characteristics of the shear-flow generator described herein are the strength and linearity of the shear flow and the low level of turbulence that can be achieved in the wind-tunnel test section. These are attributed to the design feature that any local abrupt variation of flow conditions generated from the non-uniform-porosity gauze is effectively attenuated by the downwind gauze. Instead of using the single gauze shapes in a double-gauze situation, in principle, one could modify the gauze shape first and then carry out the necessary velocity profile adjustments by changing the porosity of the first gauze. But, since changing of porosity is a relatively simple task, discrepancies in the gauze shape are not critical The theory and technique presented in this paper can be generalized to yield other desirable velocity distributions in the laboratory.

The concept of double-curved gauzes for constant-shear-flow generation was formed and tested while conducting a study sponsored by the Office of Naval Research under contract N68305-78-C-005. Special thanks are due to Dr B. Lindberg who gave valuable assistance in obtaining the numerical results presented in §4.3. Suggestions and comments of the referees which led to some extensions and revisions of this work are gratefully acknowledged.

REFERENCES

Davies, M. E. 1976 The effects of turbulent shear flow on the critical Reynolds number of a circular cylinder. *NPL Rep. Mar. Sci.* R151.

Dennis, J. E. & Schnabel, R. B. 1983 *Numerical Methods for Unconstrained Optimization and Nonlinear Equations*. Prentice-Hall.

Elder, J. W. 1959 Steady flow through nonuniform gauzes of arbitrary shape. *J. Fluid Mech.* **5**, 355.

Hardy, G. H. & Rogosinski, W. W. 1944 *Fourier Series*. Cambridge Tracts in Mathematics and Mathematical Physics No. 38. Cambridge University Press.

Kiya, M., Tamura, H. & Arie, M. 1980 Vortex shedding from a circular cylinder in a moderate-Reynolds-number shear flow. *J. Fluid Mech.* **141**, 721.

Kotansky, D. R. 1966 The use of honeycomb for shear flow generation. *AIAA J.* **4**, 1490.

LAWS, E. M. & LIVESEY, J. L. 1978 Flow through screens. *Ann. Rev. Fluid Mech.* **10**, 247.

LIVESEY, J. L. & TURNER, J. T. 1964 The generation of symmetrical duct velocity profiles of high uniform shear. *J. Fluid Mech.* **20**, 201.

MAIR, W. A. & STANSBY, P. K. 1975 Vortex wakes of bluff cylinders in shear flow. *SIAM J. Appl. Maths* **28**, 519.

MAULL, D. J. 1968 The wake characteristics of a bluff body in a shear flow. *AGARD Conf. Proc.* 48 (papers presented at the fluid dynamics panel specialists meeting held at Munich, Germany, 15–17 September 1968, paper no. 16).

MAULL, D. J. & YOUNG, R. A. 1973 Vortex shedding from bluff bodies in a shear flow. *J. Fluid Mech.* **60**, 401.

OWEN, P. R. & ZIENKIEWICZ, K. H. 1957 The production of uniform shear flow in a wind tunnel. *J. Fluid Mech.* **2**, 521.

STANSBY, P. K. 1976 The locking-on of vortex shedding due to the cross-stream vibration of circular cylinders in uniform and shear flows. *J. Fluid Mech.* **74**, 641.

TURNER, J. T. 1969 A computational method for the flow through non-uniform gauzes: the general two-dimensional case. *J. Fluid Mech.* **36**, 367.

VAHL DAVIS, G. DE 1957 Steady non-uniform flow through wire screens. Ph.D. dissertation, University of Cambridge.

WOO, H. G. C., CERMAK, J. E. & PETERKA, J. A. 1989 Secondary flows and vortex formation around a circular cylinder in constant-shear flow. *J. Fluid Mech.* **204**, 523.